

Temperature-and-filtration conditions in the embankment at the Kumtor Mine, Kyrgyzstan: Case study and contingency situation analysis

Larisa NAZAROVA⁽¹⁾, Leonid NAZAROV⁽¹⁾,
Murataly JAMANBAEV⁽²⁾ and Mirlan CHYNYBAEV⁽²⁾

(1) Institute of Mining Siberian Branch of RAS, Novosibirsk, Russia
E-mail: lanazarova@ngs.ru

(2) Razzakov Kyrgyz State Technical University, Bishkek, Kyrgyzstan

Abstract

The geomechanical model describing the heat-and-mass transfer processes in the vicinity of the protective embankment at the tailing pond of the Kumtor gold deposit (Kyrgyzstan) was designed based on the information on the structure of the object, as well as the data on thermophysical properties and permeability of frozen and thawed ground and seasonal variation of air temperature. The simulation implemented with the help of original FEM code has shown that: a) the zero isotherm between the frozen and thawed rocks attains stable location 10–15 years after the embankment creation and the pond filling; b) the decrease in the mean annual temperature essentially reduces infiltrate volume due to longer time when impermeable frozen layer covers the embankment slope surface. The inverse problem on determination of location and onset time of impervious screen damage by the data of piezometric measurements was defined. Numerical experiments revealed that the formulated problem is unambiguously resolvable at an acceptable accuracy for any real heat-transfer and filtration properties of soil if input data were recorded at a number of points and given the measurement error is moderate.

Keywords: protective embankment, heat, filtration, inverse problem

1. Introduction

Construction and operation of various purpose waterworks (protection embankment, dams, dikes, hydroelectric power plants) in permafrost zones causes natural heat disbalance, rises temperature of frozen rocks and generates new migration paths for fluid flow (Yershov and Williams, 2004; Chzhan, 2002; Vozin, 1987). This results in the instability of a waterworks structure and in pollution of environment with production waste. Various aspects of modeling of heat-mass exchange in terms of objects in permafrost areas are discussed, for instance, in (Riseborough et al, 2008; Yi et al, 2006). Substantial research deals with analyzing behavior of large natural objects over geological period of time (Bense and Person, 2008; Rawlins et al., 2009; Velicogna et al., 2012; Zhang et al., 2008) and with studying behavior of production and man-made objects (Goy et al., 1996; Lolaev et al., 1997; Buiskikh and Zamoshch, 2010).

Being the largest in Central Asia, Kumtor gold deposit was discovered in 1978 and put into operation in the mid-1990s. The deposit lies in the south-east Kyrgyzstan, in the Tian Shan mountains, at an elevation of 4 km, in the permafrost zone (www.kumtor.kg). This area belongs in the continental climate zone RF Construction norms (1996), the winter and summer temperatures are, respectively, -35°C and $+20^{\circ}\text{C}$; the mean annual temperature is 6°C (Nepomnyashchaya, 2007).

Kumtor gold ore mine uses open pit mining method, by now the mine has produced 5.6 Mt of ore with the average gold content of 3.85 g/t (www.gold-deposit.ru/2183.html). Gold is recovered by cyanidation, liquid waste goes to a tailing pond. As the tailing pond fills up, its protective embankment is built up by 1.5 m per year. At the present time, the embankment is 36 m high, the dam site is 280 m wide and its extension $Y=3$ km (Osmonbetova, 2011). To prevent slope erosion and infiltration, an impervious

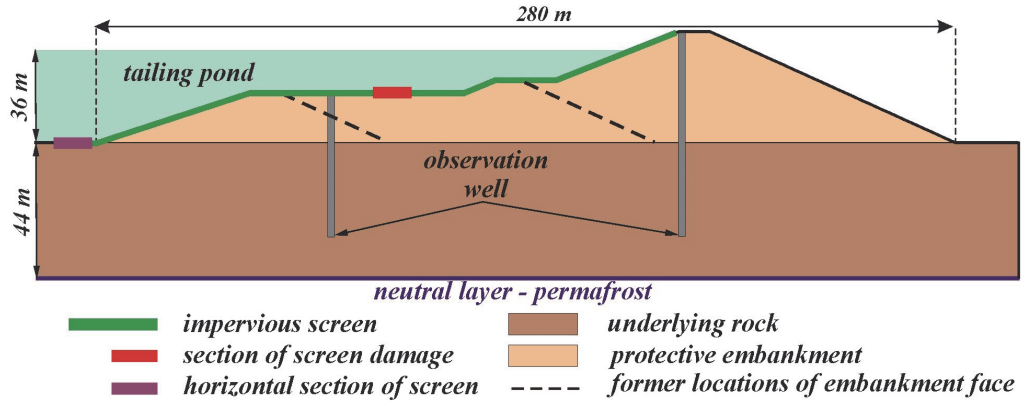


Fig. 1 Profile of the object under investigation

screen has been created: the embankment is covered with an impermeable 1.5 mm thick film that is sealed along edging (www.vb.kg/244692). The weld seals are the weakest place of the protection cover.

The temperature and filtration processes in the area of the Kumtor mine embankment and the diagnostics method for the state of the impervious screen are the subjects of the present research.

2. Formulation and solution of direct problem

Figure 1 shows structural configuration of profile of the object under analysis. The tailing pond is non-freezing over the entire service life, the fluid temperature T_w varies from 4 to 8°C. The state of the protective embankment and underlying ground is monitored by means of measuring pressure and temperature at different depth in observation boreholes.

As the extension of the object is much more than its height and width and shapes of the profiles of the embankment show a minor difference, the analysis involves a two-dimensional problem in the Cartesian coordinates (x, z) . The current state of the embankment is of the prime importance, so we simplify the situation by disregarding the change in the configuration of the embankment in the course of operation.

The lower boundary $z=Z$ of the computational domain (Fig. 2) lies in the zone of permafrost at the permanent negative temperature T_i that is accepted to equal the temperature of -2°C of the neutral layer in the discussed geographical region (RF Construction

norms, 1996). Let the embankment temperature and the underlying ground temperature $T=T_i$ at the initial time moment $t=0$, and later on the tailing pond is filled with the fluid with the temperature T_w , which is assumed constant in view of the continuity of the production process.

Thawing is much slower than the heat exchange between the fluid and the ground, therefore evolution of the temperature T is described by the transient equation of thermal conduction, considering convection (Bejan, 2013):

$$T_{,t} + \vec{V} \cdot \text{grad } T = \text{div}(k_c \text{grad } T), \quad (1)$$

where $k_c=k_c(T)$ is the thermal diffusivity coefficient; \vec{V} is the fluid flow velocity defined by the Darcy law:

$$\vec{V} = -k_s \text{grad } P / p_a, \quad (2)$$

$k_s=k_s(T)$ is the filtration coefficient; p_a is atmospheric pressure. Filtration takes place only in the thawing zone ($T>0$) where the additional pressure P obeys the equation:

$$P_{,t} = \text{div}(k_s \text{grad } P). \quad (3)$$

The boundary conditions are formulated as follows (refer to Fig. 2): at the section A_0A_1

$$T=T_w, \quad P=\rho g(z(x) - z_0) \quad (4)$$

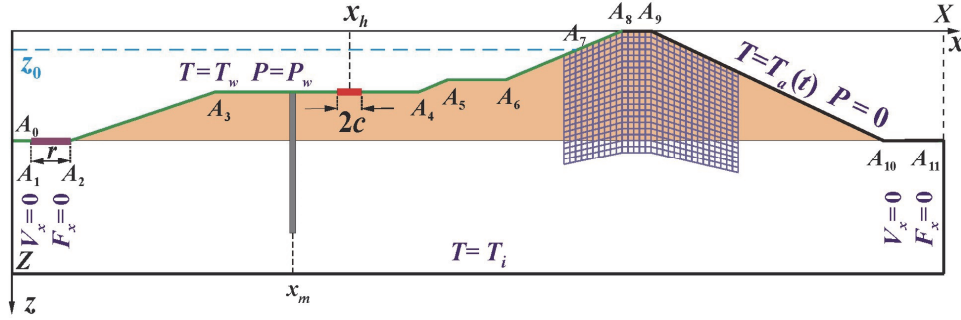


Fig. 2 Computational domain, boundary conditions and finite element mesh fragment

(ρ is the fluid density; g is the free fall acceleration; $z(x)$ is the ordinate of current boundary point); at $A_1...A_8$ (impervious screen)

$$T=T_w, \vec{V} \cdot \vec{n} = 0 \quad (5)$$

(\vec{n} is the external normal to the boundary); at the daylight surface $A_8...A_{11}$

$$T=T_a, P=0, \quad (6)$$

where $T_a = T_a(t)$ is the air temperature.

The vertical boundaries $x=0, X$ are free from the horizontal components of the velocity V_x and heat flow F_x

$$V_x=0, F_x=0; \quad (7)$$

at the boundary $z=Z$

$$T=T_i. \quad (8)$$

The system of the differential equations (1)–(3) with the boundary conditions (4)–(8) and the initial data $T(0, x, z) = T_i, P(0, x, z) = 0$ was solved using the finite element method Zienkiewicz et al. (2013) and the original codes (Nazarova, 1985; Nazarova et al., 1998). The linear size of an element was 2 m, the time step was 6 h. The calculation involved the following model parameters (Fig. 2): $X=600$ m, $Z=100$ m, $z_0=2$ m, $\rho=1020$ kg/m³. The values of the coefficients of consolidation and temperature diffusion corresponding to weakly permeable clays with medium moisture content Goncharov (2002) are compiled in the Table 1.

Table 1 Heat–filtration characteristics of rocks

Rock	$10^6 k_S, \text{ m/s}$	$10^6 k_C, \text{ m}^2/\text{s}$
Thawed	2.0	1.2
Frozen	0	2.0

Figure 3 demonstrates location of the zero isotherm (the interface of the thawed and frozen zones) at different time after filling the tailing pond at $T_w = 4^\circ\text{C}$ (blue lines) and $T_w = 8^\circ\text{C}$ (red lines).

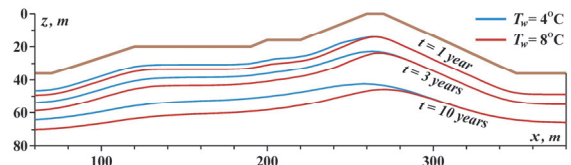


Fig. 3 Location of zero isotherm for various T_w

In the considered geographical region, the mean annual temperature is positive, therefore, the zero isotherm moves away from the upper surface and reaches the steady-state position in 10–15 years. As seen, the variation of the temperature T_w inside the production-justified range has little influence on the thawing depth.

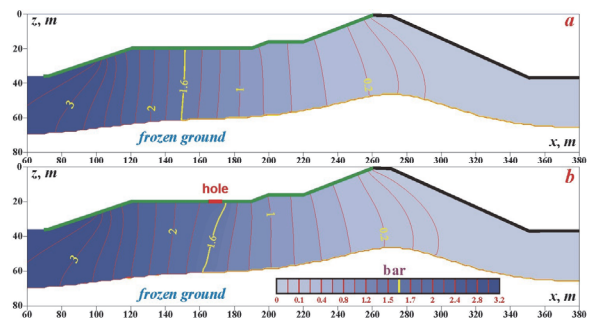


Fig. 4 Level curves of pressure (bar) 10 years after filling of the tailing pond: a) undisturbed impervious screen; b) impervious screen with rupture.

Figure 4a illustrates distribution of the pressure P at the time $t=10$ years when the length r (refer to Fig. 2) of the horizontal boundary section A_0A_1 of the impervious screen is 5 m: evidently, infiltrate reaches the surface of the right-hand slope of the protective embankment by now.

With this end in view, we analyze the influence of the value of r on the amount of infiltrate having reached the outer perimeter of the embankment $L=A_7A_8A_9A_{10}A_{11}$ (refer to Fig. 2):

$$Q(t) = Y \int_0^L \int \nabla \cdot \bar{n} dL .$$

The varicolored lines in Fig. 5 show the change in Q for different r as against $Q=Q_0$ at the time $t=10$ years when $r=0$. It appears that a comparatively slight growth of r essentially reduces the infiltrate amount and, consequently, mitigates ecological hazard.

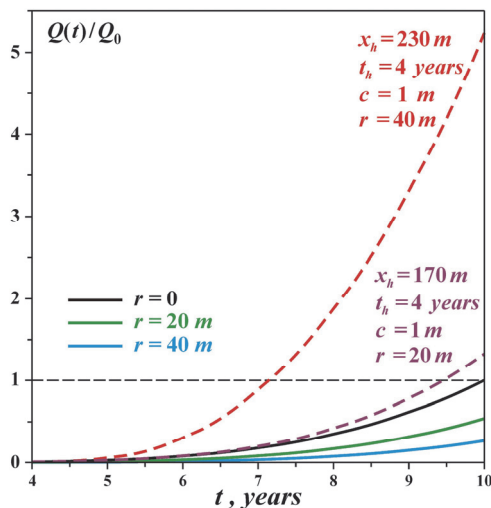


Fig. 5 Relative volume of infiltrate through embankment

The numerical experiments have shown that T_w has nearly no influence on the value of Q , while the decrease in the mean annual temperature greatly reduces the infiltrate amount due to the longer time within which the frozen layer occurs at the daylight surface of the embankment.

3. Search the location and timing of impervious screen rupture based on piezometric measurement data

To monitor the state of the protective embankment, vertical observation holes are drilled (see Figs. 1 and 2), and temperature and pressure are measured at

various depth in these holes. The temperature measurements are mainly required to monitor propagation depth of the thawing zone whereas they do not inform on the rupture of the impervious screen since the temperature is almost the same at the bottom of the tailing pond.

Let us consider how the pressure field “responds” the rupture of the impervious screen. At the time $t=t_h$ at the point $x=x_h$, due to low-quality sealing Ishchenko (2007), a hole $2c$ in length forms in the impervious screen. In this case, in the section $[x_h-c, x_h+c]$ of the upper boundary of the computational domain, the hydrostatic pressure $\rho g z_h$ is set so to be in accord with the water body depth z_h at the given point (Fig. 2). Evidently, the hole is an additional source of fluid, and the infiltration toward the daylight surface of the embankment intensifies (Fig. 4b) with closer location of the hole to the embankment surface (dashed colored lines in Fig. 5) despite the fact that the water head is twice as little at $x_h = 230$ m than at $x_h = 170$ m.

The colored lines in Fig. 6 show time variation of the pressure $P_h(t)=P(t, x_m, z_m)$ at $c=1$ m; the coordinates x_m and z_m of the observation points as well as parameters t_h and x_h of hole are specified in the insets. For the comparison, the black lines show the pressure at the same points for the undamaged impervious screen. It turns out that the pressure sensors perceive the damage of the impervious screen within the first months (depending on the distance from the damage position) to the accuracy of 10 kPa. The slope α of the curve $P_h(t)$ grows with closer distance to the hole in the screen. The behavior α is the indication of the integrity of the impervious screen.

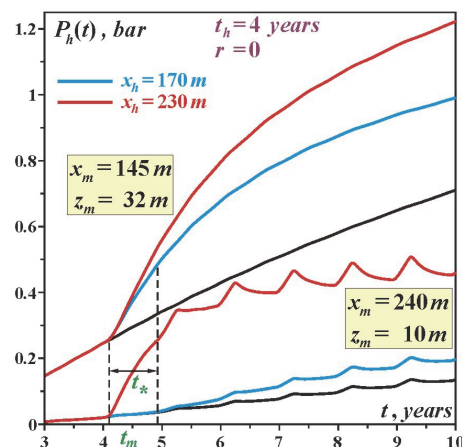


Fig. 6 Pressure at observation points for different location x_h of rupture in the impervious screen

Now, we formulate the inverse problem: search the time t_h and rupture point x_h and in the impervious screen by the data of piezometric measurements. Let introduce an objective function:

$$\Psi(t_h, x_h) = \sqrt{I(t_h, x_h) / t_* P_a}, \quad (9)$$

where

$$I(t_h, x_h) = \int_{t_m}^{t_m+t_*} [P(t, x_m, z_m, t_h, x_h) - P_*(t)]^2 dt, \quad (10)$$

The function Ψ is a dimensionless functional of discrepancy between the pressure $P_*(t)$ measured at the observation point (x_m, z_m) , that is the input data, and the “theoretical” pressure $P(t, x_m, z_m, t_h, x_h)$ at the same point, additional arguments of the function P imply that this is the direct problem (1)–(8) solution at certain values of t_h and x_h . In (9), (10) t_m is the start time of the pressure growth at the point (x_m, z_m) ; t_* is the time interval set empirically. The numerical experiments showed that t_* grows as k_3 reduces; at the chosen model parameters, $t_* = 4\text{--}6$ months.

The minimum point (t_h^*, x_h^*) of the objective function furnishes the inverse problem solution. In order to examine its resolvability, we synthesize input data:

$$P_*(t) = [1 + \delta \zeta(t)] P_0(t),$$

where $P_0(t)$ - the exact solution of the direct problem - is the pressure at the point (x_m, z_m) if the impervious screen gets ruptured at the point $x = x_h^0$ at the time $t = t_h^0$; ζ is a random variable uniformly distributed over the interval $[-1, 1]$; δ is the relative amplitude of superimposed multiplicative noise. Figures 7 and 8 show the level lines of the objective function Ψ for $\delta=0.3$, $t_*=0.5$ year, $x_h^0 = 160$ m, $t_h^0 = 4$ years for different x_m and z_m .

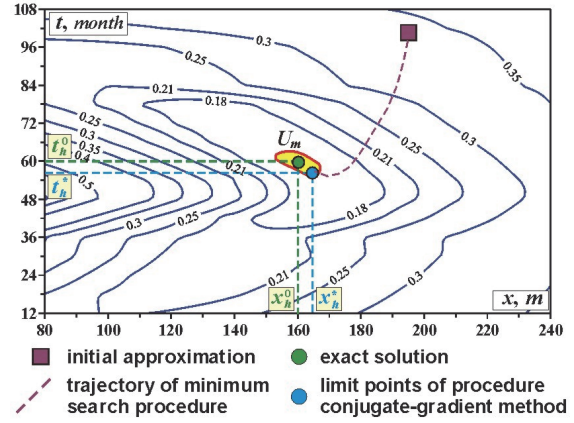


Fig. 7 Isolines of the objective function Ψ at the observation point with the coordinates $x_m=150$ m, $z_m=32$ m.

It is found that Ψ is not always unimodal (Fig. 8); for this reason, the objective functions are to be considered for various observation points.

The equivalence domain U_m (yellow-colored in Figs. 7 and 8) is a variation range of the objective function arguments such that the relative change $|\Delta\Psi|/\Psi$ is not higher than a certain small value (in our case, 0.005). The dimensions of U_m , which condition the accuracy ε of the inverse problem solution, depend on the noise level δ in the input data. The given analysis assumes $\varepsilon=0.1$, then the related value of δ is

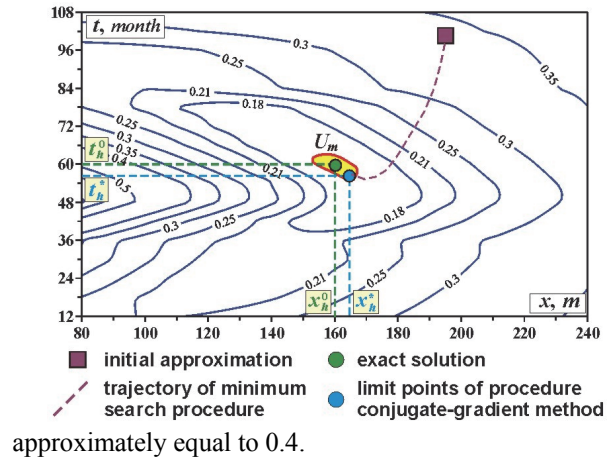


Fig. 8 Isolines of the objective function Ψ at the observation point with the coordinates $x_m=210$ m, $z_m=30$ m.

The inverse problem solution $(x_h^*, t_h^*) \in U$, where U is the intersection of the equivalence domains U_m of the objective functions constructed for a number of

points where the pressure is measured. Then, with the moderate noise in the input data, the inverse problem is unambiguously resolvable.

Based on the results of the numerical experiments, it is expedient to use gradient methods Avriel (2003), Nazarov et al. (2013) to search the minimum of Ψ if the measurement points are sufficiently distant from the frozen zone since coefficients of thermal diffusivity and filtration are discontinuous functions in the vicinity of the zero isotherm and the objective function Ψ becomes nondifferentiable as a consequence.

4. Conclusions

The authors have designed the geomechanical model describing the heat-and-mass transfer processes in the vicinity of the protective embankment at the tailing pond of the Kumtor gold deposit, Kyrgyzstan, situated in the permafrost zone. The numerical experiments have shown that: a) the zero isotherm between the frozen and thawed rocks attains stable location 10–15 years after the embankment creation and the pond filling; b) the decrease in the mean annual temperature essentially reduces infiltrate volume due to longer time when impermeable frozen layer covers the embankment slope surface; c) the change of the fluid temperature in the production-justified range has almost no influence on the depth of thawing and the amount of infiltrate in the embankment; d) a slight increase in the size of the horizontal section of the impervious screen greatly reduces the amount of infiltrate and, consequently, the pollution of the area.

The inverse problem on locating and timing a rupture of the impervious screen is unambiguously resolvable at an admissible accuracy for any real thermal and filtration characteristics of soil using the data of piezometric pressure measurements taken at a number of points and given the moderate noise in the input data.

Acknowledgements

The authors are grateful for the support provided by the Russian Foundation for Basic Researches (Project No. 14-05-90116).

References

- Avriel, M. (2003): *Nonlinear Programming: Analysis and Methods*. Dover Publishing, 532 p.
- Bejan, A. (2013): *Convection Heat Transfer*. Wiley, 4th Edition, 696 p.
- Bense, V. and Person, M. (2008): Transient hydrodynamics in inter-cratonic basins during glacial cycles, *J. Geophys. Res.*, 113, F04005.
- Buiskikh, A.A. and Zamoshch, M.N. (2010): Prediction of thermal regime within a tailing dump under permafrost, *Journal of Mining Science*, Vol. 46, No. 1, pp. 28-33.
- Chzhan, R.V. (2002): Temperature condition and stability of low-head hydraulic power systems and ground channels in permafrost zone. Yakutsk: Institute of Permafrostology SB RAS, 207 p. (in Russian)
- Goncharov, S.A. (2002): *Thermodynamics*. Moscow: Publishing House of Moscow State Mining University, 440 p. (in Russian)
- Goy, L., Fabre, D. and Menard, G. (1996): Modeling of rock temperatures for deep alpine tunnel projects, *Rock Mechanics and Rock Engineering*, Vol. 29, No. 1, pp. 1-18.
- Ishchenko, A.V. (2007): *Infiltration protection and impervious efficiency of waterworks*. Rostov-on-Don: North Caucasian Research Center of Higher School, 256 p. (in Russian)
- Lolaev, A.B., Spesivtsev, A.V., Spesivtsev, V.V. et al. (1997): Site investigation of tailing dam in permafrost region, *Geoenvironmental Engineering*. eds. R.N. Yong and H.R. Thomas. Thomas Telford, London. 657 p.
- Nazarov, L.A., Nazarova, L.A., Karchevskii, A.L., and Panov, A.V. (2013): Estimation of stresses and deformation properties of rock masses based on the solution of an inverse problem by the data of the measurement of free surface displacements, *Journal of Applied and Industrial Mathematics*, Vol. 7, No. 2, pp. 234-240.
- Nazarova, L.A. (1985): Stress state of a sloping-bedded rock mass around a working, *Journal of Mining Science*, Vol. 21, No. 2, pp. 132-135.
- Nazarova, L.A., Nazarov, L.A., and Leontiev, A.V. (1998): Three-dimensional geomechanical model of the Tashtagol iron-ore deposit, *Journal of Mining*

- Science, Vol. 34, No. 3, pp. 209-216.
- Nepomnyashchaya, T.A. (2007): Macro-zoobenthos of the Kumtor river under anthropogenic impact, KRSU Bulletin, Vol. 7, No. 1, pp. 111–113. (in Russian)
- Osmonbetova, D.K. (2011): Modern ecology in the Naryn river upstream zone and predictive estimates in view of the gold deposit development, KRSU Bulletin, Vol. 11, No. 3, pp. 50-53. (in Russian)
- Rawlins, M.A., Ye, H., Yang, D. et al. (2009): Divergence in seasonal hydrology across northern Eurasia: Emerging trends and water cycle linkages, J. Geophys. Res., 114, D18119.
- Riseborough, D., Shiklomanov, N., Etzelmuller, B. et al. (2008): Recent advances in permafrost modeling, Permafrost and Periglacial Processes, 19, pp. 137-156.
- RF Construction norms and regulations 2.01.01-82 (1996): Construction climatology and geophysics, Ministry of Construction of Russia. 140 p. (in Russian)
- Velicogna, I., Tong, J., Zhang, T. Kimball, J.S. (2012): Increasing subsurface water storage in discontinuous permafrost areas of the Lena River basin, Eurasia, detected from GRACE, Geophys. Res. Lett., 39, L09403.
- Vozin, V.F. (Ed.) (1987): Environmental impact of a hydraulic power plant in the far north. Yakutsk. 88 p. (in Russian)
- Yershov, E.D. and Williams, P.J. (2004): General geocryology. Cambridge University Press, 608 p.
- Yi, S., Arain, M.A. and Woo, M-K. (2006): Modifications of a land surface scheme for improved simulation of ground freeze-thaw in northern environments, Geophys. Res. Lett., 33, L13501.
- Zhang, Y., Chen, W., and Riseborough, D.W. (2008): Disequilibrium response of permafrost thaw to climate warming in Canada over 1850–2100, Geophys. Res. Lett., 35, L02502.
- Zienkiewicz, O.C., Taylor, R.L. and Zhu, J.Z. (2013): The Finite Element Method: Its Basis and Fundamentals. 7th Edition, Butterworth-Heinemann, 756 p.